International Journal of Biological Macromolecules 367 (2026) 152613

Contents lists available at ScienceDirect

International Journal of Biological Macromolecules

journal homepage: www.elsevier.com/locate/ijbiomac

Cellulose nanofibrils/AgNP nanostructured coating on smart packaging for indication of H_2O_2 in milk

Kelcilene B.R. Teodoro [a,b,*], Thalita J. Bondancia [a,b], Rafaela C. Sanfelice [c,d], Débora T. Balogh [d], Aurore Denneulin [a], Daniel S. Correa [b], Luiz H.C. Mattoso [b,**], Julien Bras [a,e]

[a] University Grenoble Alpes, CNRS, Grenoble INP, LGP2, 38000, Grenoble, France
[b] Nanotechnology National Laboratory for Agriculture (LNNA), Embrapa Instrumentation, 13560-970, São Carlos, SP, Brazil
[c] Institute of Technological Sciences (ICT), Federal University of Alfenas (Unifal-MG), Brazil
[d] São Carlos Institute of Physics, University of São Paulo, São Carlos, SP, Brazil
[e] Institut Universitaire de France (IUF), 75000, Paris, France

ARTICLE INFO

Keywords:
Colorimetric sensor
Nanoparticles
Nanocellulose
Coating
Hydrogen peroxide

ABSTRACT

Colorimetric sensors offer user-friendly means of analysis, and do not require wired connections or antennas. These attributes make them suitable for integration into intelligent packaging systems, which enables real-time monitoring of product quality throughout the production and logistics chain, extending to the end consumer. Here we developed colorimetric sensors for detecting H_2O_2 adulteration in milk with a simple and cost-effective approach. Specifically, the sensor was manufactured using paper and can be adapted for use as labels or seals for commercial packaging. A nanohybrid formulation comprising TEMPO-oxidized cellulose nanofibrils and silver nanoparticles (AgNP) was used to modify the paper surface via bar coating technique. Nanocellulose acted as a stabilizer and nucleating site for the synthesis of AgNP and facilitated the homogeneous deposition of the nanohybrid formulation onto the paper. Applying CNF/AgNP improved the paper's roughness and porosity, resulting in homogeneous samples with stable optical properties. The developed platform demonstrated visible bleaching in the presence of H_2O_2 within a concentration range of 100 μM to 1 mM, with a detection limit of 74 μM, good selectivity against common interfering molecules found in milk, and suitable response in recovery tests using whole, semi-skimmed and skimmed milk, demonstrating its potential for real samples analysis.

1. Introduction

The latest United Nation report (World Population Prospects 2019) highlights a significant population surge projected until the year 2050, estimating that the global population will reach 9.7 billion by this time, necessitating a corresponding 60% increase in food production [1,2]. Therefore, issues regarding food supply and quality are expected to be one of the important challenges to be overcome in this scenario [3]. Innovative technologies incorporated to food packaging can directly contribute to the safety and quality of food for suppliers and consumers, providing protection, containment, transmission of information, and marketing details [4,5]. It is expected that the packaging materials should meet these specific requirements, however, novel studies in the field have reported the possibility to provide additional functions to packaging, as is the cases of active packaging [6–8] and smart (also called intelligent) packaging [9–12]. Smart packages aim to transmit information about the conservation status of food through devices such as sensors and biosensors, capable of monitoring the environment inside the packaging [6,11,13,14].

The detection of specific compounds or parameters of interest (analytes) to the food industry and the consumers can help monitoring food quality and safety, potentially reducing food losses and wastes, and protecting consumer health. [15] detection This task can be achieved by integrating electrical devices [16,17] or by incorporating specific dyes or optically active nanomaterials into the packaging materials [4,18,19]. Using the latter enables the design packaging associated to easy-to-interpret optical sensors, facilitating the detection of analytes. Optical sensors can detect varied changes in the optical properties of materials such as color, absorbance, fluorescence, reflectance, and refractive index to monitor different analytes [20–22].

* Correspondence to: K.B.R. Teodoro, University Grenoble Alpes, CNRS, Grenoble INP, LGP2, 38000, Grenoble, France.
** Corresponding author.
E-mail addresses: kbr.teodoro@gmail.com (K.B.R. Teodoro), luiz.mattoso@embrapa.br (L.H.C. Mattoso).

https://doi.org/10.1016/j.ijbiomac.2026.152613
Received 3 February 2026; Received in revised form 5 May 2026; Accepted 18 May 2026
Available online 19 May 2026

A compound of significant concern in food detection is hydrogen peroxide (H_2O_2), widely utilized across pharmaceutical, medical, cosmetics, and food industries for its potential bactericidal and sporicidal properties [23]. The intentional addition of this compound in dairy products, such as milk, has been a fraudulent tactic, employed with the intent of enhancing preservation, extending the shelf life and maximizing profitability [24,25]. Specifically, the inclusion of this substance in food products can lead to a reduction of its nutritional content, damaging vitamins A and E, and its recurring consumption may have adverse effects on the overall health of the population, including diabetes, cancer and cardiovascular disorder [26,27] Therefore, colorimetric sensor for H_2O_2 detection has arisen as an alternative to traditional electrochemistry, fluorescence, chemiluminescence, and other laboratorial approaches that require specific specialists and proper

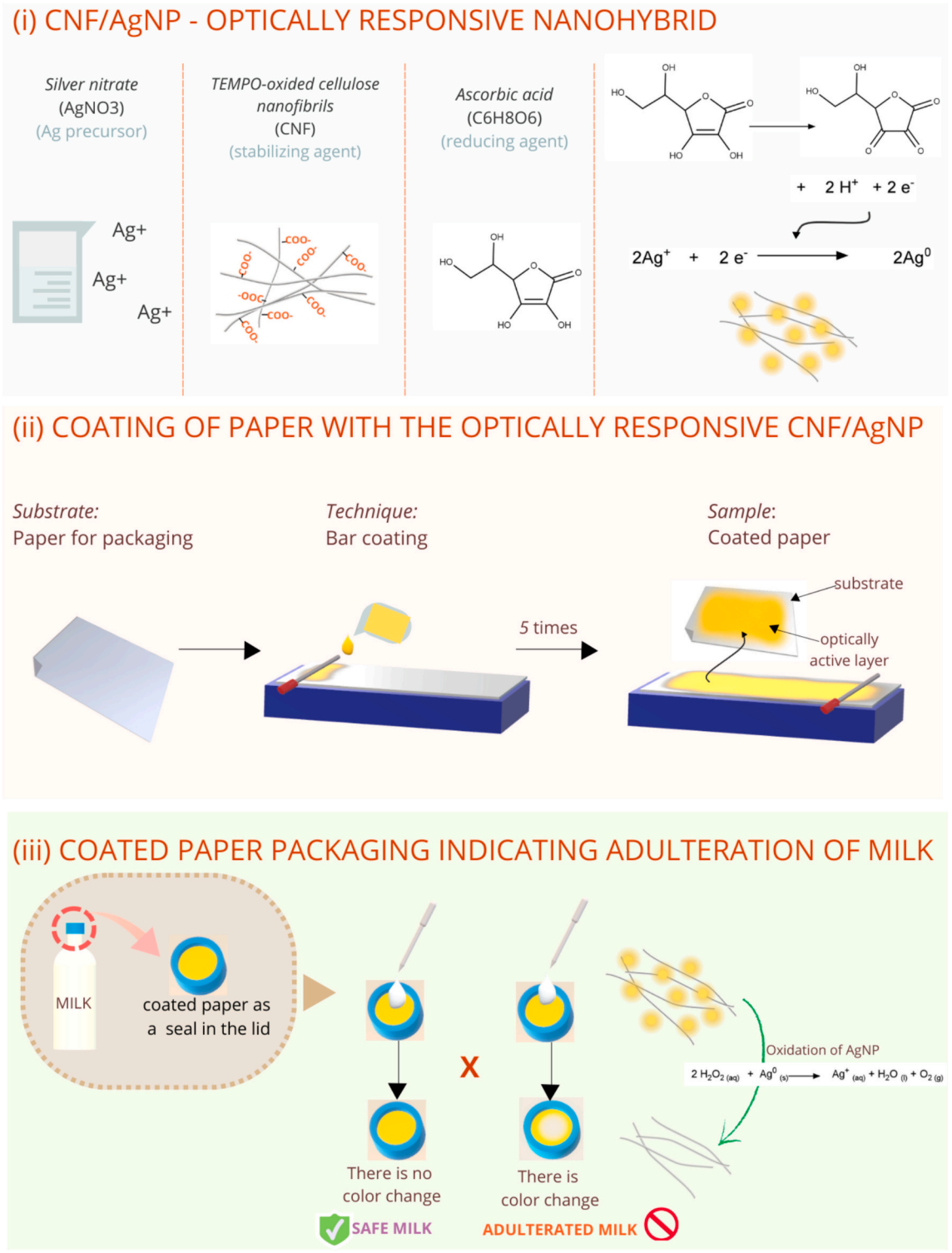

Scheme 1. – Schematic representation of the following steps: (i) green synthesis of the nanohybrid CNF/AgNP using $AgNO_3$ as silver precursor, CNF as stabilizing agent, and ascorbic acid as reducing agent; (ii) fabrication of the paper-based optical sensor combining the nanohybrid CNF/AgNP and packaging paper via the bar coating technique; and (iii) the application of the optical sensors for colorimetric detection of H_2O_2 in milk, with the proposal of application as seals in milk lids.

instrumentations [20,23].

Scientific studies investigating morphological modifications in systems containing metallic nanoparticles such as gold, silver, platinum, and their alloys, demonstrate the affordability and effectiveness of colorimetric systems for detecting H_2O_2 in milk [24,25,28,29] For instance, the specific interactions between H_2O_2 and AgNP permits H_2O_2 detection by electrochemical and spectrophotometric techniques [29–31]. One issue is the production of AgNP and their deposition onto substrate. Recently, an efficient strategy to include these nanomaterials into smart packaging consists in the combination with nanocelluloses (NC) (including nanofibrils (CNF), cellulose nanocrystals (CNC) or bacterial celluloses (BC)), favoring the replacement of conventional additives toward sustainability [32,33]. One key advantage is that NC can play simultaneously the role of nucleating agent for AgNP production and the role of stabilizer and rheological additive adapted for coating.

An effective approach to address practical challenges associated with packaged products involves employing coating technique, resulting in the formation of thin additional layers on the package surface [34,35]. The utilization of NC as a nanostructured coating agent has garnered significant attention in recent research endeavors [36–40]. The aim of applying NC as coating onto paper surfaces is to create a thin layer of fine particles that coat the rough and porous irregularities [41]. The use of nanocelluloses enables surface smoothing of papers by filling gaps, but mainly it helps a very homogeneous spreading of compounds like pigments, binders, thickeners, crosslinkers, optical brightening agents (OBA), lubricants, and improving printability [33,35]. It has been proved that the use of NC optimizes the dispersion and helps having similar properties than other coating but with far fewer particles. For instance, using CNF and TiO_2 dispersion improve opacity with using 50% less pigment than classic coating with TiO_2. Specially for paper packaging, the use of NC provides strong hydrogen bonded interactions and uniform coating [35] with a good adhesion and barrier properties which can protect the particles. Besides, NC have recently been employed by authors in sensors, acting as disposable substrates, support for nano and biohybrids in the manufacture of electrical, electrochemical, optical, piezoelectric and other types of chemical sensors [20]. Despite such interest, up to our knowledge, no study has investigated formulations combining nanocellulose and AgNP for milk characterization.

In this direction, here we harness the potential of CNF and AgNP nanohybrids (CNF/AgNP) to create a water-based, optically responsive suspension for depositing onto paper packaging via bar coating technique, as illustrated in Scheme 1 (i) and ii). Papers modified with CNF/AgNP were evaluated for their colorimetric response to H_2O_2 in milk (Scheme 1 – iii), showcasing their potential application as labels, seals or other components in food commercial packaging. Rather than functioning as a standalone analytical indicator, the proposed sensing system was designed to be integrated into packaging formats (e.g., labels or tamper-evident seals on bottle caps), enabling direct and user-friendly monitoring of product quality throughout storage and consumption.

2. Materials and methods

2.1. Materials

TEMPO-oxidized cellulose nanofibrils (CNF) were obtained from Nippon Paper Group. Silver nitrate ($AgNO_3$) was purchased from Thermo-Fisher and the ascorbic acid used was purchased from Sigma. Paper substrate (Gerbier ®) was provided by an industrial partner (Ahlstrom). This is a classic paper specially designed to be coated. It was stored at least 24 h in 50% RH and 23 °C before any use. Distilled water was used for any formulations.

2.2. CNF/AgNP nanohybrid

2.2.1. Synthesis of CNF/AgNP nanohybrid

For the synthesis of CNF/AgNP, the AgNP were produced following chemical reduction method [42], using ascorbic acid as the reducing agent [43], and the CNF as the stabilizing agent [43,44]. To an aqueous suspension of CNF at 1 wt%, 10 mg of $AgNO_3$ was added and allowed to interact with CNF for 2 h. Next, 80 μL of a 0.3 M ascorbic acid aqueous solution was slowly dripped onto the suspension. The synthesis was performed under ambient temperature and vigorous stirring. A color change from translucent to bright yellow was observed at the end of the procedure. The final suspension was kept under stirring for 2 h and stored in refrigerator.

2.2.2. CNF/AgNP nanohybrid characterization

The CNF/AgNP nanohybrid was characterized regarding their physicochemical properties using transmission electron microscopy (TEM), Fourier transform infrared spectroscopy (FTIR), and UV–Vis absorption spectroscopy (UV–Vis). The TEM analysis was performed using a Philips CM 200/FEI (USA) Transmission Electron Microscope (TEM) equipped with a TemCam F216 from TVIPS (Germany), working at 200 kV acceleration voltage. For this, the CNF and CNF/AgNP suspensions were diluted and dripped on a copper grid with an amorphous carbon coating, and stained with uranyl acetate (2%). At least 2 samples and 10 TEM images were obtained for each sample. The most representative image was selected for discussion.

A Spectrum 1000 Perkin-Elmer spectrometer equipped with attenuated total reflection apparatus (ATR) was used to obtain the FTIR spectra. FTIR spectra were obtained in transmittance mode, in the range 4000–400 cm^{-1}, using 32 scans and resolution of 2 cm^{-1}. Triplicate measurements were performed for each sample and the most representative spectra were selected for the discussions.

The optical properties of CNF/AgNP nanohybrid were evaluated by UV–Vis spectroscopy (UV-1600 spectrometer Shimadzu spectrometer, software UV Probe 2.31), monitoring the typical AgNP band in the region of 410 nm to 430 nm, and the samples were placed in a 1 cm optical path quartz cell and ultrapure water was used as blank. Minimum triplicate measurements were performed and average is used for discussions.

2.3. CNF/AgNP sensing layer fabrication by bar coating

2.3.1. Functionalization of paper packaging with CNF/AgNP by bar coating

The prepared CNF/AgNP aqueous suspension (1 wt%) was used to coat commercial packaging paper (matte side of paper) using the bar coating technique as previously described by co-authors [40]. The coating was carried out on an RK Control Coater machine, equipped with two different wired bars (Meyer bars): a thinner 0.15 mm wire bar, and a thicker 1.27 mm wire bar. The different bars are able to produce coating layers with different thicknesses, related with the amount of material spread on the substrate surface. The thinner wire bar was initially used with the aim of forming a thin layer of CNF/AgNP for surface smoothening, filling the spaces between paper fibers, while the thicker bar was used for deposition of higher amount of CNF/AgNP and providing more intense color. In this way, the deposition of five layers was carried where the first layer was deposited using the red bar, and the following ones (second to fifth layers) were made with the blue bar. The deposition steps were performed with a fixed coating speed of 5 m min^{-1}, followed by oven drying step of 5 min at 80 °C. The deposition of five layers was chosen as an optimal trade-off between signal intensity and material efficiency, providing a strong optical response while minimizing nanomaterial consumption. After each deposition step, the samples were dried in a convection oven at 80 °C for 5 min. The drying of each layer was verified qualitatively by visual inspection (absence of surface gloss) and by gentle contact with a flat spatula to ensure the absence of tackiness before applying the subsequent layer. The selected

drying time represents a compromise between efficient solvent removal and process practicality, and was found to be sufficient for complete drying of the thin coating layers.

2.3.2. Coated paper characterization

The deposition effects of active layers on packaging paper were investigated by analyzing differences in the grammage, thickness, roughness, and porosity, following the classic standard procedures as described by coauthors' work [36] Before grammage measurements, the samples (n = 10) were conditioned at a temperature of 25 °C, and relative humidity of 50%, for 24 h. The effect of CNF/AgNP deposition on the non-coated and coated paper grammage was evaluated accordingly to the ISO standard 536:2019, measuring the basic weights on a digital scale (Shimadzu AUW220, ± 0.00001 g of precision) and calculating the average using 10 specimens. The specimen's thickness cross-sections of the non-coated and coated papers were evaluated using field emission scanning electron microscopy (FESEM). For this, small pieces of the coated paper were placed on stubs and coated with platinum. Ten images of different regions were used, and the measurements were performed using ImageJ software.

Differences in roughness were evaluated using optical profilometry and atomic force microscopy (AFM). The profilometry was conducted using an Alicona optical profilometer, 20× lens, and ten regions were analyzed. The average is used for the discussions. The AFM analysis was carried out with a Nanosurf AFM system, in tapping mode, analyzing five regions of each specimen (2 cm^2) placed onto glass slides. The surface of the coated paper was also investigated by FESEM analysis, using LEI and COMPO mode. For this, small pieces of the coated paper were placed on stubs and coated with platinum. The influence of the layers' deposition onto the paper packaging color was investigated using Diffuse Reflectance Spectroscopy (UV-DR) (Shimadzu UV-2600). The measurements were performed in reflectance mode, using barium sulfate as blank, and five specimens from each sample were evaluated.

2.4. H_2O_2 sensing experiments

The experiments for H_2O_2 were performed by dripping the tested solutions on the coated side of the five-layered coated paper. H_2O_2 aqueous solutions were prepared in ultrapure water, varying the concentrations in the range from 100 μM (0.1 mM) to 1 mM. Aliquots of 200 μL of each H_2O_2 aqueous solution were dripped on the coated papers, let to interact during 10 min, then the solution was removed and the specimens were dried with air jets. Absorbance spectra were obtained using a HR2000 Ocean Optics portable spectrophotometer, from 200 to 1100 nm, coupled with a QR600–7-SR125BX optical fiber. Background spectra were recorded against a completely white surface, before the addition of H_2O_2, and after the drying step. From these data, three linear calibration curves were obtained by monitoring the absorbance at 410 nm, and the limits of detection (LoD) were calculated from five measurements of the absorbances after addition of 100 μM H_2O_2 concentration.

In order to evaluate the sensor selectivity and application to real samples analysis, interferents tests (using compounds commonly found in milk matrices, such as glucose, sodium citrate, urea, and calcium) and with three types of milks (whole, semi-skimmed, and skimmed) were applied for validation of the proposed sensor for real samples. For the tests with real samples, the milks were diluted 100× in ultrapure water and spiked with 1 mM H_2O_2 concentration.

3. Results and discussion

3.1. CNF/AgNP nanohybrid characterization

In this work, the nanocellulose used for nanohybrid synthesis was a commercially obtained TEMPO-oxidized CNF. As our starting material, the TEMPO-oxidized CNF was characterized in terms of morphology and chemical composition. Besides the techniques applied for the nanohybrid characterization, which were also applied for the starting material, for comparison effects, the TEMPO-oxidized cellulose nanofibrils (CNF) were also characterized solid-state ^{13}C NMR spectroscopy. The TEM image (Fig. 1A) reveals that the starting material is composed of nanocellulose, which are arranged in a dense and homogeneous network of long, highly entangled nanofibrils with nanoscale diameters and high aspect ratio, which are typical features of CNF produced via TEMPO-mediated oxidation followed by fibrillation [45,46]. Fig. 1B demonstrates the normal distribution of the data related to the measurements of nanostructures: CNF diameters and CNF length, and AgNP diameters. The micrograph depicts the typical flexible fibril morphology of TEMPO-oxidized CNF [47]. The average dimensions of CNF were measured as 127 ± 31 nm for length and 4.6 ± 1 nm for diameter (n = 100). The solid-state 13C NMR spectrum (Fig. 1C) confirms the chemical structure of oxidized cellulose, showing well-resolved signals assigned to the glucopyranose ring carbons: C1 at 105 ppm; C2, C3, and C5 at 72 and 75 ppm, C4 at 84 and 89 ppm, and C6 at 63 and 65 ppm, along with the presence of a characteristic signal at 175 ppm corresponding to carboxylate (C=O) groups. The surface modification by TEMPO oxidation is a highly regioselective procedure of cellulose oxidation that promotes the conversion of the primary hydroxyl groups at C6 into carboxyl groups [48], reflecting in the signal in 175 ppm.

The morphological characterization of the CNF/AgNP nanohybrid prepared was carried out using the TEM technique, resulting in the micrographs shown in Fig. 1D. The AgNP obtained using TEMPO-oxidized CNF as stabilizing agent and ascorbic acid as reducing agent showed spherical aspect, with average diameters of 22 ± 9 nm. This is in accordance with the previous works using nanocellulose as a nucleating structure for silver nanoparticles [29,44,49]. The ^{13}C NMR spectrum of the CNF/AgNP nanohybrid was compared with that of pristine CNF (Fig. 1C), showing no significant differences in peak positions or profiles. This indicates that the incorporation of AgNP does not alter the chemical structure of the CNF, confirming its role as a stabilizing and supporting matrix rather than a chemically modified component.

The composition of the CNF/AgNP nanohybrid was investigated by FTIR and UV–Vis spectroscopies. The FTIR spectra of CNF/AgNP, CNF and ascorbic acid, are shown in the Fig. 1E. The nanohybrid spectrum mainly consists in cellulose band assignments, and this spectrum was analyzed according to Foster and coworkers protocol and additional references [47,50,51]. For both CNF and CNF/AgNP were found bands corresponding to the stretching vibrations of the O—H bonds of primary and secondary hydroxyl groups (3000–3700 cm^{-1}), C—H bonds were indicated by the signal centered in 2900 cm^{-1}, and the small signals at 1720 cm^{-1} indicate the presence of surface carbonyl groups. The adsorbed water molecules led to bands assigned at 1600 cm^{-1} for CNF and 1635 cm^{-1} for CNF/AgNP, as well as at 400 and 700 cm^{-1}. The region between 1470 and 1315 cm^{-1} corresponds to in-plane bending vibration bands caused by the primary and secondary OH groups. The band at 1160 cm^{-1} is related to to the C–O–C glycosidic bond antisymmetric stretching vibration, and the C—O bond of carbons 2, 3 and 6 vibrations were denoted by bands in 1110, 1060 and 1035 cm^{-1}, while at 880 cm^{-1} was assigned to hemiacetal from β-glucopyranose ring. Out of plane hydrogen bonded O—H torsional vibrations were assigned at 665 and 705 cm^{-1}, and the other bands below 800 cm^{-1} correspond to C—C bonds vibrations. The main differences between the spectra occurred between 1750 and 1500 cm^{-1}, where an overall decrease was observed, as well as a decrease in the bands at 1641 cm^{-1} and 1613 cm^{-1} and a slight increase in the band at 1592 cm^{-1}. Considering that these bands are related to surface phenomena, such as the presence of carboxyl groups and adsorbed water, these changes may indicate possible changes with AgNP.

The concentration of the aqueous nanohybrid suspension, determined by gravimetry, yielded 1.0 wt%, corresponding to 10 mg mL^{-1}. The UV–Vis spectrum in Fig. 1F shows the main absorption bands in the visible range 400–430 nm, corresponding to the typical surface plasmon

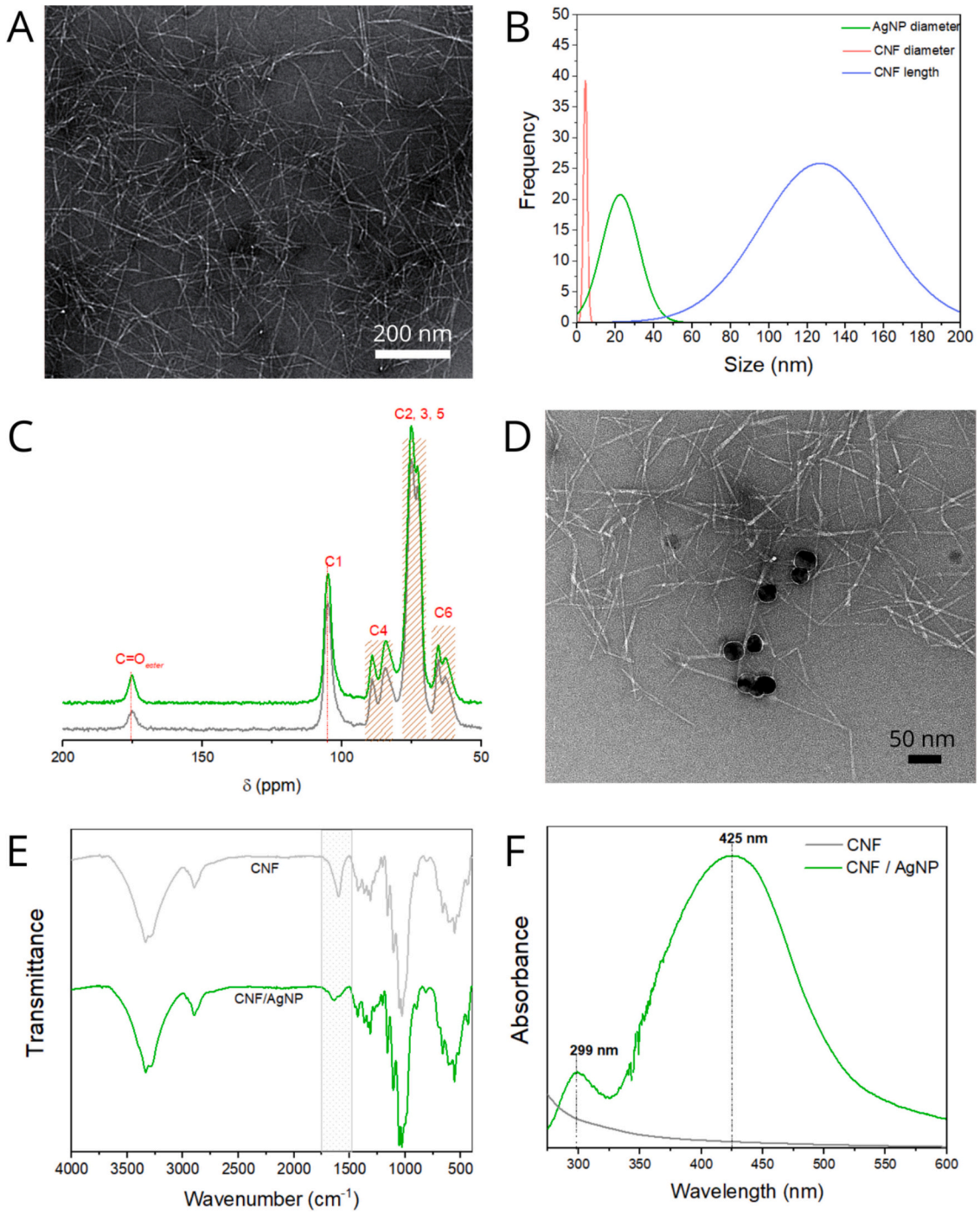

Fig. 1. – (A) TEM image of the commercial TEMPO-oxidized CNF used in this work as starting material. (B) Solid-state ^{13}C NMR spectra of the TEMPO-oxidized CNF and CNF/AgNP nanohybrid. (C) TEM image of CNF/AgNP. (D) Histograms of AgNP diameter distribution, CNF diameter and length distributions ($n = 100$). (E) FTIR spectra of CNF and CNF/AgNP. (F) UV–Vis spectra of neat CNF and CNF/AgNP.

resonance (SPR) of spherical AgNP [42,52] It was also observed the UV–Vis absorption band attributed to cellulose, at 299 nm [53] Absorption peaks at around 270 and 300 nm correspond to alcohol, ether, and hydrocarbon groups joined by aliphatic bonds [54], and has been attributed to the absorption peak to the acetal groups in cellulose [54,55]. It is noteworthy that the pristine CNF only displays certain optical activity at these shorter wavelengths, confirming that the optical response in the visible region arises exclusively from the presence of AgNP.

CNF have a surface rich in hydroxyl groups (-OH), when oxidized by the TEMPO method, these hydroxyl groups are partially converted into carboxylic groups (-COOH), which present increased negative surface charge density [47]. These functional groups on the CNF surface can strongly interact with silver ions and AgNP, primarily through chemical bonding mechanisms, such as electrostatic interactions, or coordination with metal ions [56] In the synthesis of silver nanoparticles, ascorbic acid acts as a strong reducing agent, reducing silver ions to metallic silver in the presence of CNF. During this process, the carboxyl groups on the CNFs can complex with the silver ions, facilitating their localized reduction, yielding the formation of AgNP on the CNF surface. This results in effective hybridization, where the CNFs not only stabilize but also direct the nucleation and growth of the AgNP. Additionally, the

presence of carboxylic groups on the CNF surface makes them excellent stabilizing agents for AgNP. These groups can bind to the silver ions, reducing them to metallic silver while simultaneously preventing the agglomeration of the formed nanoparticles. This interaction not only stabilizes the AgNP but also can control the size and distribution of the nanoparticles [57,58] Furthermore, the synergistic interaction between CNF and AgNP in the nanohybrid results in unique properties. For example, the combination of suitable mechanical and biodegradable properties of CNF with the antimicrobial and conductive properties of AgNP can lead to applications in areas such as active packaging, biomedical devices, and sensors. The fibrillar and highly entangled structure of CNFs, which is capable of forming conformable networks, [59,60]contributed with the effective dispersion of AgNPs, helping to stabilize and spatially distribut nanoparticles.

3.2. Coated paper characterization

Considering the aim of this study was to develop a colorimetric sensor able to indicate H_2O_2 presence in milk samples, the number of layers was determined by the color visual intensity caused by the CNF/AgNP layer deposition. The influence of the CNF/AgNP layers on the color of the paper packaging was investigated by UV-DR spectroscopy. The relation of the absorbance values with the number of layers is shown in Fig. 2 A. The absorbance increase follows the number of layers increase, as a consequence of the presence of more CNF/AgNP nanohybrid in the sample. A very intense color could be reached with five layers of CNF/AgNP, eliminating the necessity of additional layers. It confirms the advantage of nanocellulose for a homogeneous dispersion of nanoparticle. The short standard deviations associated to the measurements can be an indicative of the homogeneity of the deposition. The suitable distribution of the AgNP is verified by FESEM micrograph images displayed in Fig. 2 (B) and (C), which reveal bright points related to the presence of AgNP. The analysis was performed in lower (Fig. 2 (B) 250 ×) and higher magnifications (Fig. 2 (C) 20,000 ×), where the latter was obtained using back-scattering electrons, which make AgNP shinner dots in the corresponding image.

Specimens containing one and five layers were characterized, and the physical aspect of the final sample (five layers) is shown in the Scheme 1 (ii). The effect of each layer reflected on slight increase in grammage, from 54.7 ± 0.9 g m^2 for neat paper, to 57. 6 ± 0.8 g m^2 for the paper coated with five layers of CNF/AgNP. From zero to five layers, an increase of 5% in the weight of the packaging paper was observed. The small standard deviation suggests homogeneity in deposition. The effects of deposition on paper thickness were evaluated by SEM images displayed in the Fig. 3. Fig. 3 A shows the SEM image of the paper packaging substrate cross-section, while Fig. 3 B shows the SEM image of the paper coated with five layers of CNF/AgNP cross-section. The corresponding thickness average value of the thin coating layer, measured in 15 distinct points, was 0.85 ± 0.2 μm. An increase of thickness for the five-layers coating is observed, associated to a higher standard deviation, which indicates the presence of regions with lower deposition and regions with more deposited material. The surface morphology of paper

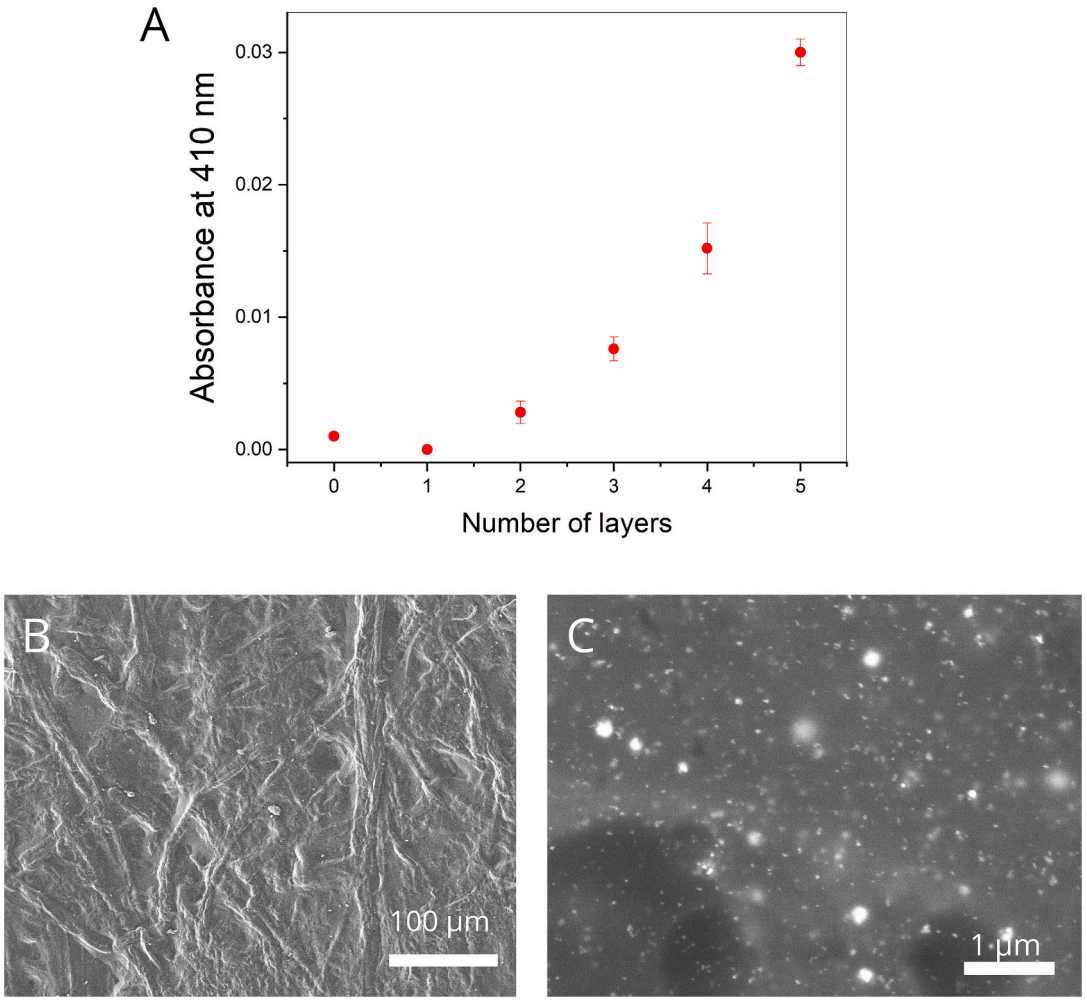

Fig. 2. – (A) Absorbance values versus number of layers on the papers' samples. FESEM micrograph images in LEI mode (B) (250 × magnification) and COMPO mode (C) (back-scattering, 20,000 × magnification) of the five layered coated paper.

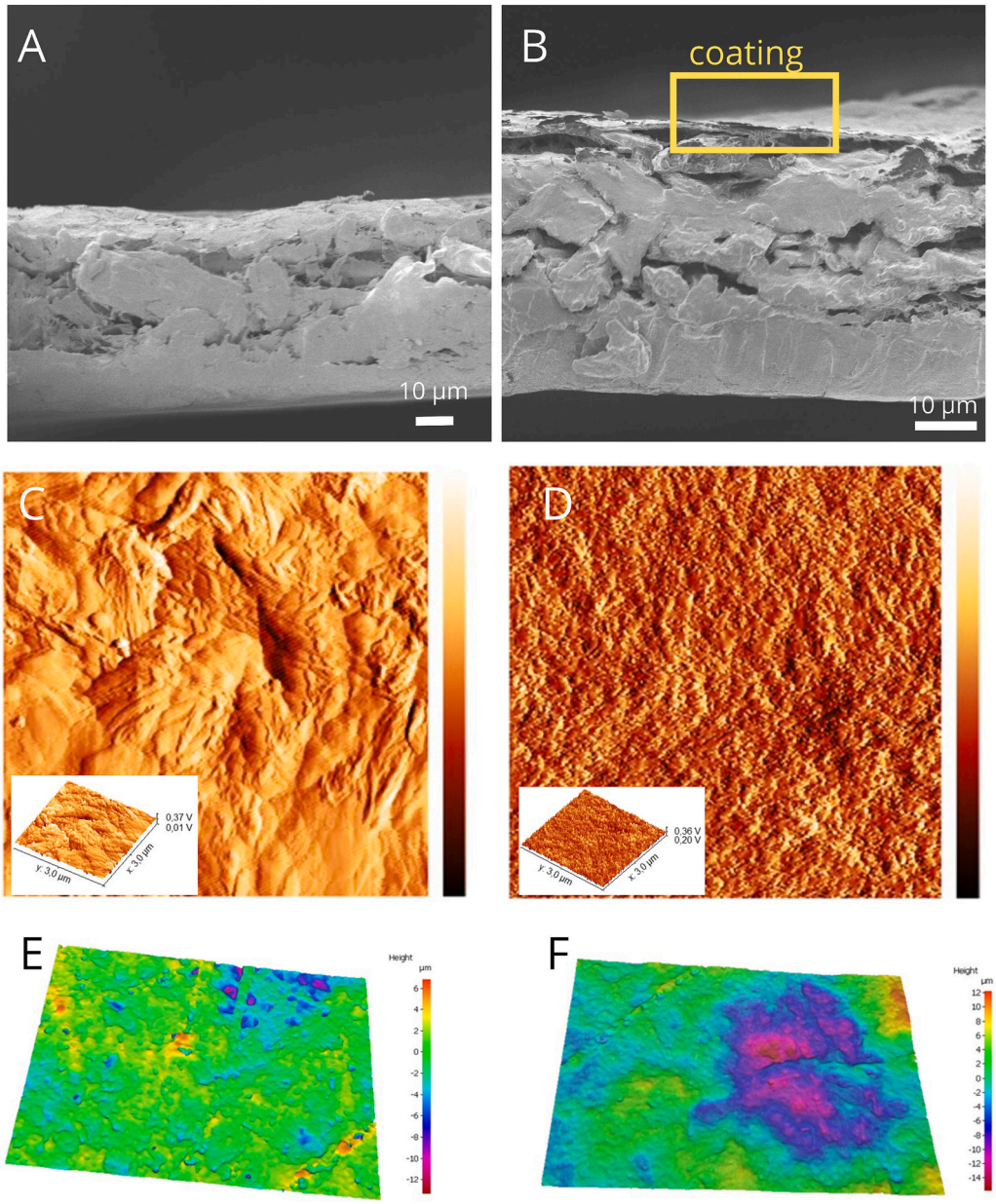

Fig. 3. – Morphological analysis of the uncoated and coated paper (five layers), respectively. FESEM micrograph images of the cross-section (A-B), surface topography obtained by AFM analysis (C—D), where the insets correspond to the 3D image of the same region. (*E*-F) are the surface profiles obtained by profilometry.

coated with five active layers of CNF/AgNP was investigated using AFM and profilometry technique, which provides visual information regarding the paper surface roughness. The topographic diagrams shown in Fig. 3 (C – F) show the differences in the topography of the original packaging paper surface and the surface coated with five CNF/AgNP active layers. Fig. 3 (C) and (D) show the 2D AFM images, and in the insets are the 3D images of the same region. In Fig. 3 (E – F) are displayed diagrams of the profilometry analysis. The root mean square roughness (Rq) decreased from 975.3 ± 67 nm ($n = 3$) for the uncoated paper to 694.7 ± 121 nm after coating (n = 3), indicating a significant reduction in fine-scale surface irregularities. Both techniques showed that, after the deposition of five layers of CNF/AgNP, an evident decrease in roughness and the mapping of regions with lower heights are verified, indicating that the deposition of the nanocellulose-based material was able to provide surface uniformity for the paper, suggesting improvements in the smoothness aspect.

3.3. Colorimetric detection of H_2O_2

For colorimetric detection experiments, different concentrations of H_2O_2 (from 100 μM to 1 mM) were dripped onto the paper modified with 5 layers of CNF/AgNP nanohybrid. The sensitivity of the colorimetric system was then evaluated by monitoring the absorbance at 410 nm, whose values decreased as a consequence of the H_2O_2 concentration increase, as shown in Fig. 4 A. The calibration curve representing the absorbance values versus H_2O_2 concentration is shown in Fig. 4 B, and displayed good linearity ($R^2 = 0.997$). The corresponding paper's color change from yellowish to white (as the H_2O_2 increased) can be seen in digital pictures shown in Fig. 4 C.

The limit of detection (LoD) was calculated based on the standard deviation (σ) of the colorimetric response at 410 nm (using the measurements of five replicates), and the angular coefficient (S) of the calibration curve, according to LoD = 3.3 σ/S [61], yielding 0.074 mM. The performance of the CNF/AgNP coated paper for sensing H_2O_2 was

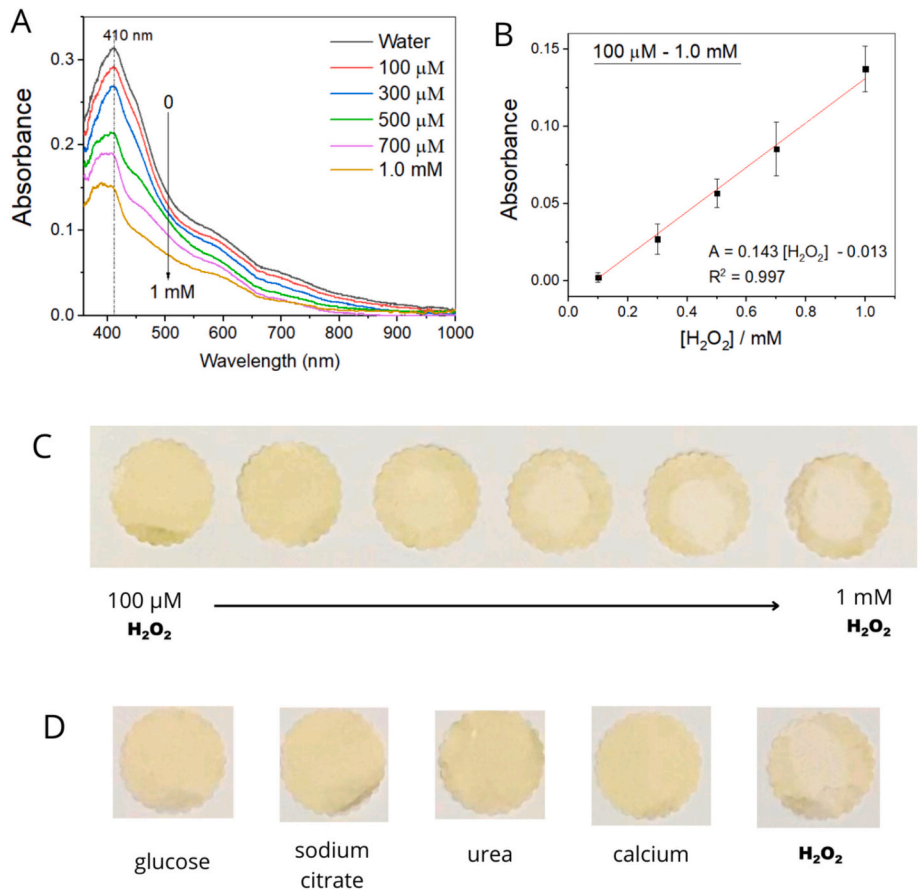

Fig. 4. – Colorimetric detection of H_2O_2 using the CNF/AgNP coated paper. (A) UV–Vis reflectance spectra in the presence of different concentrations of the H_2O_2 (100 μM– 1 mM) (B) Linear response of the colorimetric assay versus H_2O_2 concentration. (C) Digital photograph of the coated paper exposed to different H_2O_2 concentrations. (D) Selectivity test for the colorimetric sensor in the presence of distinct interferents (glucose, sodium citrate, urea, and calcium), where only the sample containing H_2O_2 became colorless.

compared to other investigations reported in literature, and is described in Table 1.

Besides, the interference effect of coexisting compounds typically found in milk over H_2O_2 detection was evaluated by selectivity test using glucose, sodium citrate, calcium, urea. The results can be observed in Fig. 4 D, where the interfering compounds were not able to cause color changes in the coated paper. In contrast, H_2O_2 clearly led to a bleaching effect, confirming the efficiency of CNF/AgNP coated paper as a selective sensing platform for H_2O_2. In order to validate the applicability of the proposed sensing platform in real analyses of H_2O_2 in milk, the sensor response was evaluated towards whole, semi-skimmed and skimmed milk samples spiked with 1.0 mM H_2O_2 solution. Recovery rates reported as 116% for whole milk, 114% for semi-skimmed milk, and 112% for skimmed milk were obtained, which indicate the potential of the CNF/AgNP nanocoating for developing intelligent packaging towards H_2O_2 detection in different types of milk samples.

Table 1
– Comparison of analytical performance of different paper-based platforms for colorimetric sensing of H_2O_2.

Type of sensing platform	LoD (mol L^{-1})	Range (mol L^{-1})	Color change	References
Bioactive paper	11.8×10^{-4}	12.5×10^{-4} to 150×10^{-4}	White to red	[25]
Starch-iodide-gelatin	1×10^{-4}	0.5×10^{-6} to 6×10^{-3}	White to dark blue	[62]
Cellulose nanofibrils/ carbon dots / TMB (nanozyme)	0.93 and 1.73×10^{-6}	6×10^{-6} to 42×10^{-6} and 10×10^{-6} to 70×10^{-6}	White to blue	[63]
Silver nanoparticles/ sericine/TMB (nanozyme)	4×10^{-3}	1.5×10^{-3} to 7.0×10^{-1}	White to blue	[64]
Paper with AgNP reduced by spent coffee grounds	1.3×10^{-3}	3.0×10^{-2} to 1.7×10^{-1}	Yellow to white	[65]
Paper with Au@Ag nanorods	1.0×10^{-4}	1.0×10^{-4} to 1.0×10^{-2}	Orange-brown to white	[66]
Packaging paper coated with CNF/AgNP	7.4×10^{-5}	1×10^{-4} to 1×10^{-3}	Yellow to white	This work

A detailed analysis of the spectra associated to the calibration curve is displayed in Fig. 5. The typical bands of AgNP in the region of 400–450 nm is verified, however, it is also observed the presence of other wider bands in the region of 500–700 nm. The band centered at 410 nm corresponds to the SPR phenomenon, which occurs when electrons on the metal nanoparticles surface oscillate in response to incident electromagnetic field [67,68] For AgNP, the SPR band usually appears between 390 nm and 420 nm, depending on the size, shape, dielectric environment, and degree of agglomeration of the nanoparticles [68] The bands displayed in Fig. 5 (B), around 410 nm, suggests AgNP of relatively small size and with little agglomeration level. On the other hand, the presence of the bands around 580 nm, showed in Fig. 5 (C), may indicate the formation of AgNP aggregates or the presence of nanoparticles with anisotropic shapes (such as nanorods or nanoprisms), which exhibit longer surface plasmon resonance modes [44,49,69] AgNP, when aggregated or with non-spherical shapes, can display

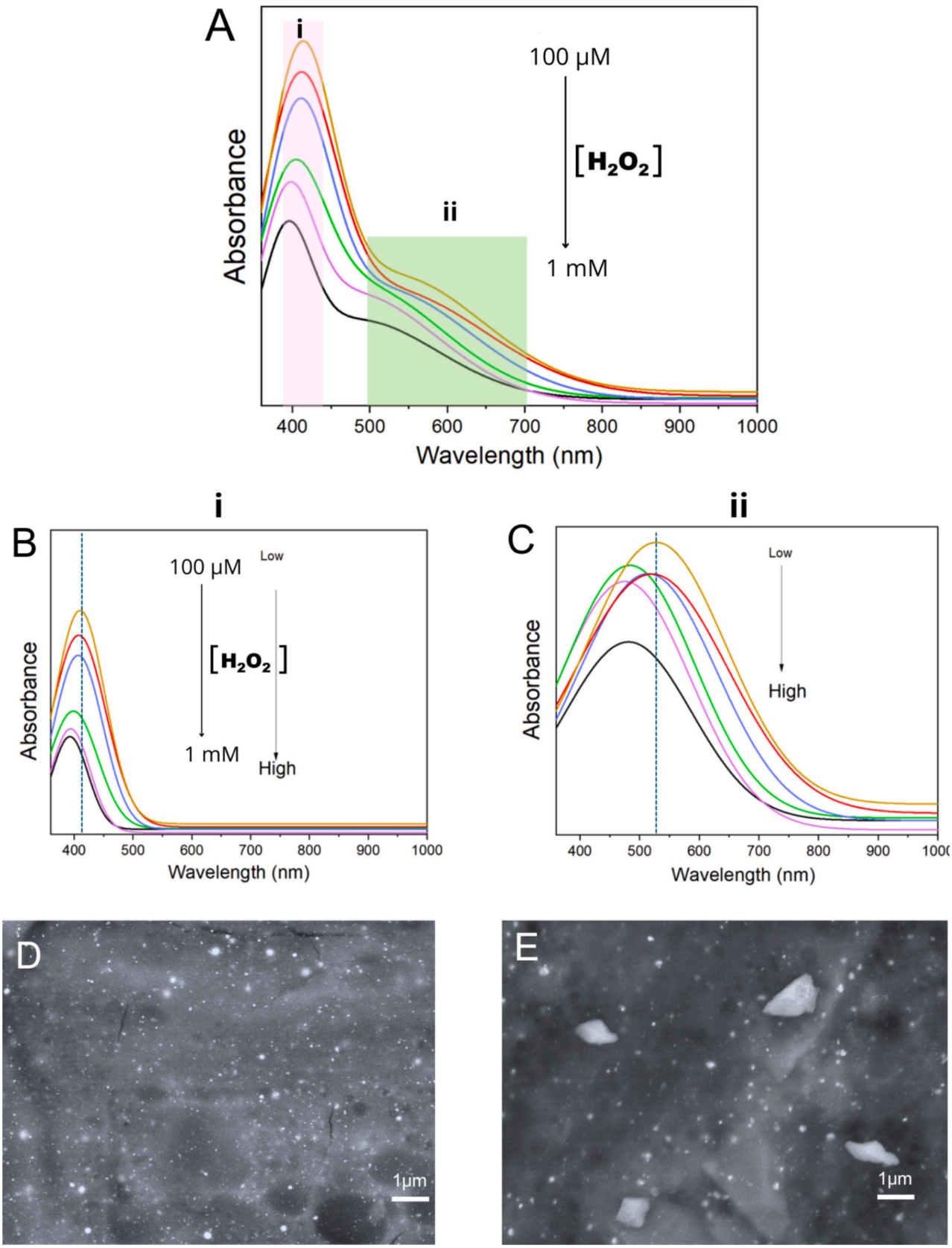

Fig. 5. – Deconvolution of the UV–Vis spectra for every spectrum of the calibration curve (100 μM to 1 mM of H_2O_2). In (A) there are the total spectra, indicating the regions of deconvolution: (i) between 400 and 450 nm, and (ii) between 500 and 700 nm. The deconvoluted bands of the region i (pink color) is shown in (B), and of the region ii (green color) is shown in (C). In (D) is shown the FESEM micrographs of the coated paper before (D) and after (E) addition of H_2O_2 obtained in COMPO mode (backscattered electrons).

plasmonic interactions that lead to shifts in absorption to longer wavelengths. The FESEM micrographs of the coated paper before and after addition of H_2O_2 is shown in Fig. 5 (D) and (E), respectively. Comparing these images, it is observed the presence of few agglomerates before addition of H_2O_2, while larger clusters are observed for the sample that has been in contact with H_2O_2, accompanied by a visible decrease of the small bright points that indicate well-dispersed AgNP. These morphological differences can be associated to the gradual changes on the absorbance spectral bands.

Upon the addition of H_2O_2 to the paper containing AgNP and CNF, a decrease in the intensity of the band centered at 410 nm is observed, along with a slight shift towards shorter wavelengths. For the band centered around 580 nm, the shift to shorter wavelengths is much more pronounced. This phenomenon can be explained by the oxidative effect of H_2O_2 on the AgNP. H_2O_2 acts as an oxidizing agent, potentially altering the surface chemistry of the AgNP. The decrease in the intensity of the band at 410 nm suggests partial oxidation and possibly the dissolution of smaller nanoparticles, leading to a reduction in the overall density of free electrons available for surface plasmon resonance. This reduction in electron density diminishes the SPR effect, thereby decreasing the intensity of the absorption band. The more pronounced shift to shorter wavelengths for the band at 580 nm suggests significant changes in the particle aggregation state or shape. The presence of H_2O_2 may lead to etching or reshaping of the AgNP, affecting their plasmonic interactions. As the nanoparticles become less aggregated or more spherical due to oxidative etching, their plasmonic peak shifts to reflect the altered optical properties [70]. These shifts and changes in band intensity are indicative of the dynamic interactions between H_2O_2 and the AgNP, revealing insights into the sensitivity of the CNF/AgNP composite to oxidative environments, which could be valuable for applications in sensing technologies. Moreover, changes in the dielectric environment surrounding the nanoparticles, such as changes in the CNF matrix or the presence of other chemical compounds, can also contribute to affecting the position and intensity of the SPR bands.

4. Conclusions

A paper-based colorimetric sensor for H_2O_2 detection in milk samples was successfully developed by coating commercially available packaging paper with a CNF/AgNP nanohybrid. The film deposition of five layers led to a slight alteration in paper's grammage and thickness, and improved smoothness and porosity. The nanostructured sensing platform exhibited a clear colorimetric response (from yellowish to white) towards H_2O_2 detection, good linearity ($R^2 = 0.997$) over 100 μM - 1 mM, and a limit of detection of 74 μM. The selectivity test showed that the coated paper did not suffer remarkable color changes in the presence of interfering compounds present in milk, yielding recovery rates of 116%, 114%, and 112% when tested in whole, semi-skimmed and skimmed milk samples, respectively. These results highlight that the CNF/AgNP-coated paper has potential to be used as labels or seals for intelligent packaging applications in food quality monitoring. Importantly, the sensor is conceived as an on-package indicator rather than a separate test device, supporting real-time quality tracking and consumer-level access within intelligent packaging systems.

CRediT authorship contribution statement

Kelcilene B.R. Teodoro: Writing – review & editing, Writing – original draft, Visualization, Validation, Project administration, Methodology, Investigation, Formal analysis, Data curation, Conceptualization. **Thalita J. Bondancia:** Writing – review & editing, Writing – original draft, Validation, Methodology, Formal analysis. **Rafaela C. Sanfelice:** Writing – review & editing, Writing – original draft, Visualization, Validation, Methodology, Formal analysis. **Débora T. Balogh:** Validation, Methodology, Formal analysis. **Aurore Denneulin:** Writing – review & editing, Writing – original draft, Resources, Funding acquisition, Data curation, Conceptualization. **Daniel S. Correa:** Writing – review & editing, Writing – original draft, Resources, Funding acquisition, Data curation, Conceptualization. **Luiz H.C. Mattoso:** Writing – review & editing, Writing – original draft, Supervision, Resources, Project administration, Funding acquisition, Conceptualization. **Julien Bras:** Writing – review & editing, Writing – original draft, Supervision, Resources, Project administration, Funding acquisition, Conceptualization.

Declaration of competing interest

The authors declare no conflicts of interest.

Acknowledgements

The authors thank the financial support from Conselho Nacional de Desenvolvimento Científico e Tecnológico (CNPq) (120289/2025-3, 200589/2022-9, 200590/2022-7), MCTI-SisNano, Coordenação de Aperfeiçoamento de Pessoal de Nível Superior - Brasil (CAPES) (Financing Code 001), FAPESP (2018/22214-6, 2023/01567-6) and Rede Agronano-EMBRAPA from Brazil. Part of the work have been done in the LGP2 (France) thanks to Erasmus+ Traineeship Program. The LGP2 is part of the LabEx Tec 21 (Grant Agreement No. ANR-11-LABX-0030), the Institut Carnot PolyNat (Grant Agreement No. ANR-16-CARN-002501) and the Cross disciplinary program Glyco@Alps (Investissements d'avenir – Grant agreement ANR-15-IDEX-02).

Data availability

Data will be made available on request.

References

[1] Department of Economic and Social Affairs Population Division, World population prospects 2019, in: World Population Prospects 2019, 2019. Number 141.
[2] M.S. Gumisiriza, J.M.L. Kabirizi, M. Mugerwa, P.A. Ndakidemi, E.R. Mbega, Can soilless farming feed urban East Africa? An assessment of the benefits and challenges of hydroponics in Uganda and Tanzania, Environ. Chall. 6 (August 2021) (2022) 100413, https://doi.org/10.1016/j.envc.2021.100413.
[3] B.G. Martini, G.A. Helfer, J.L.V. Barbosa, R.C. Espinosa Modolo, M.R. da Silva, R. M. de Figueiredo, A.S. Mendes, L.A. Silva, V.R.Q. Leithardt, IndoorPlant: A model for intelligent Services in Indoor Agriculture Based on context histories, Sensors 21 (5) (2021) 1631, https://doi.org/10.3390/s21051631.
[4] Y. Chang, M.D. Ferreira, D.S. Correa, K.B.R. Teodoro, F.R. Procopio, R.P. Brexó, A. Sarkhosh, J.K. Brecht, Advances in postharvest nanotechnology: enhancing fresh produce shelf life and quality to reduce losses and waste, Postharvest Biol. Technol. 222 (2025) 113397, https://doi.org/10.1016/j.postharvbio.2025.113397.
[5] S. Haider, N. Mirza, M. Anwar-ul-Haq, K. Bibi, V. Munyaneza, A. Ali, I.A. Ahmed, M. Mehran, S. Sohail, A. Zafar, D. e Zainab, S. Rauf, Nanoencapsulation approaches in food processing and packaging, in: Nanotechnology Innovations for Food Security and Sustainable Agriculture, Wiley, 2026, pp. 357–383, https://doi.org/10.1002/9781394349012.ch14.
[6] N.H. Azman, W.M. Khairul, N.M. Sarbon, A comprehensive review on biocompatible film sensor containing natural extract: active/intelligent food packaging, Food Control 141 (January) (2022) 109189, https://doi.org/10.1016/j.foodcont.2022.109189.
[7] S. Gao, D.J. McClements, B. Wang, A. Rashid, X. Geng, S. Sun, W. Wang, H. Hou, Regulation of mechanical and barrier properties of starch/PBAT films from extrusion perspective: structural evolution, correlation insights, and predictive model development, ACS Sustain. Chem. Eng. 13 (43) (2025) 18776–18794, https://doi.org/10.1021/acssuschemeng.5c07433.
[8] S. Jancikova, D. Dordevic, K. Tesikova, B. Antonic, B. Tremlova, Active edible films fortified with natural extracts: case study with fresh-cut apple pieces, Membranes 11 (9) (2021), https://doi.org/10.3390/membranes11090684.
[9] M.M. Calabretta, D. Gregucci, R. Desiderio, E. Michelini, Colorimetric paper sensor for food spoilage based on biogenic amine monitoring, Biosensors 13 (1) (2023), https://doi.org/10.3390/bios13010126.
[10] N. Halonen, P.S. Pálvölgyi, A. Bassani, C. Fiorentini, R. Nair, G. Spigno, K. Kordas, Bio-based smart materials for food packaging and sensors – A review, Front. Mater. 7 (April) (2020) 1–14, https://doi.org/10.3389/fmats.2020.00082.
[11] H. Nawaz, T. Liang, Y. Wang, A. He, Z. Wu, X. Ning, Y. Jiang, A.K. Alanazi, J. Zhang, F. Xu, Cellulose-derived excitation wavelength-dependent Ultrastrong and smart films for smart packaging applications, ACS Appl. Polym. Mater. 7 (24) (2025) 17142–17153, https://doi.org/10.1021/acsapm.5c04153.

[12] C. Rodrigues, V.G.L. Souza, I. Coelhoso, A.L. Fernando, Bio-based sensors for smart food packaging—current applications and future trends, Sensors 21 (6) (2021) 2148, https://doi.org/10.3390/s21062148.
[13] B. Chen, M. Zhang, H. Chen, A.S. Mujumdar, Z. Guo, Progress in smart labels for rapid quality detection of fruit and vegetables: a review, Postharvest Biol. Technol. 198 (January) (2023), https://doi.org/10.1016/j.postharvbio.2023.112261.
[14] S. Gao, S. Sun, J. Zhao, W. Wang, H. Hou, A biodegradable pH-response packaging film with blueberry extract: blown-extrusion fabrication, multifunctional activity, and kinetic investigation, Food Chem. 449 (2024) 139217, https://doi.org/10.1016/j.foodchem.2024.139217.
[15] B. Kuswandi, M. Moradi, P. Ezati, Food sensors: off-package and on-package approaches, Packag. Technol. Sci. 35 (12) (2022) 847–862, https://doi.org/10.1002/pts.2683.
[16] H.M.C. Azeredo, D.S. Correa, Smart choices: mechanisms of intelligent food packaging, Current Research in Food Science 4 (2021) 932–936, https://doi.org/10.1016/j.crfs.2021.11.016.
[17] A. Tirkey, P.J. Babu, Sensors and actuators for food packaging, in: Smart and Intelligent Food Packaging, Elsevier, 2026, pp. 29–49, https://doi.org/10.1016/B978-0-443-24724-8.00011-9.
[18] P. Sakare, S.K. Giri, D. Mohapatra, B. Modhera, V.B. Babu, Lac dye-based intelligent colorimetric indicator for real-time freshness monitoring of packaged white button mushrooms (*Agaricus bisporus*), Postharvest Biol. Technol. 206 (July) (2023) 112552, https://doi.org/10.1016/j.postharvbio.2023.112552.
[19] J. Shen, Q. Liu, R. Zhang, Z. Zhang, Q. Chen, J. Ning, L. Li, Integration of colorimetric sensing dyes and multi-substrate arrays for food quality and safety monitoring: design, optimization, and analysis, Compr. Rev. Food Sci. Food Saf. 25 (1) (2026), https://doi.org/10.1111/1541-4337.70344.
[20] K.B.R. Teodoro, R.C. Sanfelice, F.L. Migliorini, A. Pavinatto, M.H.M. Facure, D. S. Correa, A review on the role and performance of cellulose nanomaterials in sensors, ACS Sens. 6 (7) (2021) 2473–2496, https://doi.org/10.1021/acssensors.1c00473.
[21] D. Yan, R. Li, W. Lu, C. Piao, L. Qiu, Z. Meng, S. Wang, Flexible construction of cellulose photonic crystal optical sensing nano-materials detecting organic solvents, Analyst 144 (6) (2019) 1892–1897, https://doi.org/10.1039/c8an01236a.
[22] S. Zhang, J. Ye, Y. Sun, J. Kang, J. Liu, Y. Wang, Y. Li, L. Zhang, G. Ning, Electrospun fibrous mat based on silver (I) metal-organic frameworks-polylactic acid for bacterial killing and antibiotic-free wound dressing, Chem. Eng. J. 390 (January) (2020) 124523, https://doi.org/10.1016/j.cej.2020.124523.
[23] P. Sangkaew, A. Ngamaroonchote, Y. Sanguansap, K. Karn-orachai, Emerging electrochemical sensor based on bimetallic AuPt NPs for on-site detection of hydrogen peroxide adulteration in raw cow Milk, Electrocatalysis 13 (6) (2022) 794–806, https://doi.org/10.1007/s12678-022-00763-1.
[24] A. Karimi, S.W. Husain, M. Hosseini, P.A. Azar, M.R. Ganjali, Rapid and sensitive detection of hydrogen peroxide in milk by enzyme-free electrochemiluminescence sensor based on a polypyrrole-cerium oxide nanocomposite, Sens. Actuators B 271 (2018) 90–96, https://doi.org/10.1016/j.snb.2018.05.066.
[25] L.S. Lima, E.L. Rossini, L. Pezza, H.R. Pezza, Bioactive paper platform for detection of hydrogen peroxide in milk, Spectrochim. Acta A Mol. Biomol. Spectrosc. 227 (2020) 117774, https://doi.org/10.1016/j.saa.2019.117774.
[26] C.A. Juan, J.M. Pérez de la Lastra, F.J. Plou, E. Pérez-Lebeña, The chemistry of reactive oxygen species (ROS) revisited: outlining their role in biological macromolecules (DNA, lipids and proteins) and induced pathologies, Int. J. Mol. Sci. 22 (9) (2021) 4642, https://doi.org/10.3390/ijms22094642.
[27] R.T. Vargas, P.V.D. Andrade, M.M.O.P. Cerqueira, F.N. Souza, J.R. Guimarães, C. V. Guimarães Ladeira, M.M. Melo, E.J. Facury Filho, H.M. Brandão, A.D. S. Guimarães, Influence of reactive oxygen and nitrogen species on udder health and milk quality, Revista Do Instituto de Laticínios Cândido Tostes 76 (2) (2022) 131–141, https://doi.org/10.14295/2238-6416.v76i2.851.
[28] M. Buzdar, A. Yaqub, A. Hayat, M.Z. Ul Haq, A. Khan, H. Ajab, Paper based colorimetric sensor using novel green magnetized nanocomposite of pinus for hydrogen peroxide detection in water and milk, Food Biosci. 55 (July) (2023) 103014, https://doi.org/10.1016/j.fbio.2023.103014.
[29] K.B.R. Teodoro, F.L. Migliorini, W.A. Christinelli, D.S. Correa, Detection of hydrogen peroxide (H_2O_2) using a colorimetric sensor based on cellulose nanowhiskers and silver nanoparticles, Carbohydr. Polym. 212 (February) (2019) 235–241, https://doi.org/10.1016/j.carbpol.2019.02.053.
[30] M. Farrokhnia, S. Karimi, S. Momeni, S. Khalililaghab, Colorimetric sensor assay for detection of hydrogen peroxide using green synthesis of silver chloride nanoparticles: experimental and theoretical evidence, Sens. Actuators B 246 (2017) 979–987, https://doi.org/10.1016/j.snb.2017.02.066.
[31] S. Majhi, R. Singh, C.S.P. Tripathi, D. Guin, In situ synthesis of carbon quantum dots@gum Arabic-silver nanoparticles as a "turn off-on" dual fluorescent probe for rapid detection of hydrogen peroxide and mercury (II) ions in aqueous media, New J. Chem. (2024), https://doi.org/10.1039/D4NJ00798K.
[32] F. Hoeng, J. Bras, E. Gicquel, G. Krosnicki, A. Denneulin, Inkjet printing of nanocellulose–silver ink onto nanocellulose coated cardboard, RSC Adv. 7 (25) (2017) 15372–15381, https://doi.org/10.1039/C6RA23667G.
[33] L. Spagnuolo, R. D'Orsi, A. Operamolla, Nanocellulose for paper and textile coating: the importance of surface chemistry, ChemPlusChem 87 (8) (2022), https://doi.org/10.1002/cplu.202200204.
[34] E.C. Lengowski, E.A. Bonfatti Júnior, L. Coelho Simon, G.I. Bolzon de Muniz, A. Sulato de Andrade, A. Neves Leite, E.L. Souza de Miranda Leite, Nanocellulose coating on Kraft paper, Coatings 13 (10) (2023) 1705, https://doi.org/10.3390/coatings13101705.
[35] A. Li, D. Xu, L. Luo, Y. Zhou, W. Yan, X. Leng, D. Dai, Y. Zhou, H. Ahmad, J. Rao, M. Fan, Overview of nanocellulose as additives in paper processing and paper products, Nanotechnol. Rev. 10 (1) (2021) 264–281, https://doi.org/10.1515/ntrev-2021-0023.
[36] E. Gicquel, C. Martin, J. Garrido Yanez, J. Bras, Cellulose nanocrystals as new bio-based coating layer for improving fiber-based mechanical and barrier properties, J. Mater. Sci. 52 (6) (2017) 3048–3061, https://doi.org/10.1007/s10853-016-0589-x.
[37] M.A. Herrera, A.P. Mathew, K. Oksman, Barrier and mechanical properties of plasticized and cross-linked nanocellulose coatings for paper packaging applications, Cellulose 24 (9) (2017) 3969–3980, https://doi.org/10.1007/s10570-017-1405-8.
[38] A. Mazega, Q. Tarrés, R. Aguado, M.À. Pèlach, P. Mutjé, P.J.T. Ferreira, M. Delgado-Aguilar, Improving the barrier properties of paper to moisture, air, and grease with Nanocellulose-based coating suspensions, Nanomaterials 12 (20) (2022) 3675, https://doi.org/10.3390/nano12203675.
[39] S. Roy, L. Zhai, L. Van Hai, J.W. Kim, J.H. Park, H.C. Kim, J. Kim, One-step nanocellulose coating converts tissue paper into an efficient separation membrane, Cellulose 25 (9) (2018) 4871–4886, https://doi.org/10.1007/s10570-018-1945-6.
[40] H. Spieser, A. Denneulin, D. Deganello, D. Gethin, R. Koppolu, J. Bras, Cellulose nanofibrils and silver nanowires active coatings for the development of antibacterial packaging surfaces, Carbohydr. Polym. 240 (2020) 1–23, https://doi.org/10.1016/j.carbpol.2020.116305.
[41] Q. Wang, N. Ding, Coating factors influencing the fold cracking of coated papers, Nord. Pulp Pap. Res. J. 35 (3) (2020) 419–431, https://doi.org/10.1515/npprj-2019-0051.
[42] Y.A. Krutyakov, A.A. Kudrinskiy, A.Y. Olenin, G.V. Lisichkin, Synthesis and properties of silver nanoparticles: advances and prospects, Russ. Chem. Rev. 77 (3) (2008) 233–257, https://doi.org/10.1070/RC2008v077n03ABEH003751.
[43] N.P.U. Nguyen, N.T. Dang, L. Doan, T.T.H. Nguyen, Synthesis of silver nanoparticles: from conventional to 'modern' methods—A review, Processes 11 (9) (2023) 2617, https://doi.org/10.3390/pr11092617.
[44] K.B.R. Teodoro, R.C. Sanfelice, L.H.C. Mattoso, D.S. Correa, Cellulose whiskers influence the morphology and antibacterial properties of silver nanoparticles composites, J. Nanosci. Nanotechnol. 18 (7) (2018) 1–8, https://doi.org/10.1166/jnn.2018.15285.
[45] Y.N. Asfira, Holilah, D. Prasetyoko, R.F. Faradilla, Asranudin, A.W. Pratama, Z.A. A. Hamid, B. Piluharto, M.S.A. Rani, E.P. Ramdhani, L. Suryanegara, M.N. F. Norrrahim, A.Z. Aini, Isolation and physicochemical characterization of TEMPO-oxidized cellulose nanofibers from edamame husk (*Glycine max* L. Merrill) and their use in composite membranes, Biomass Bioenergy 209 (2026) 108915, https://doi.org/10.1016/j.biombioe.2025.108915.
[46] Nippon Paper Industries Co., Ltd., Nippon Paper Industries Succeeds in Practical Application of Cellulose Nanofiber by TEMPO Catalytic Oxidation, 2015. , April 21, Https://Www.Nipponpapergroup.Com/English/News/Year/2015/News150421003061.Html.
[47] E.J. Foster, R.J. Moon, U.P. Agarwal, M.J. Bortner, J. Bras, S. Camarero-Espinosa, K.J. Chan, M.J.D. Clift, E.D. Cranston, S.J. Eichhorn, D.M. Fox, W.Y. Hamad, L. Heux, B. Jean, M. Korey, W. Nieh, K.J. Ong, M.S. Reid, S. Renneckar, J. Youngblood, Current characterization methods for cellulose nanomaterials, Chem. Soc. Rev. 47 (8) (2018) 2609–2679, https://doi.org/10.1039/c6cs00895j.
[48] R. Gusain, U. Chaudhary, V. Rana, G. Joshi, P.K. Gupta, R.K. Bachheti, L.A. Worku, Transforming cellulose for sustainability: comprehensive insights into modification approaches and their applications, ACS Omega (2026), https://doi.org/10.1021/acsomega.5c07738.
[49] K.B.R. Teodoro, R.C. Sanfelice, L.H.C. Mattoso, D.S. Correa, Cellulose whiskers influence the morphology and antibacterial properties of silver nanoparticles composites, J. Nanosci. Nanotechnol. 18 (2018) 4876–4883, https://doi.org/10.1166/jnn.2018.15285.
[50] K.S. Lefroy, B.S. Murray, M.E. Ries, T.D. Curwen, A natural, cellulose-based microgel for water-in-oil emulsions, Food Hydrocoll. 113 (April 2021) (2021) 106408, https://doi.org/10.1016/j.foodhyd.2020.106408.
[51] K.B.R. Teodoro, M.H.M. Facure, R. Schneider, A.D. Alvarenga, R.S. Andre, D. S. Correa, Self-standing thin films of cellulose nanocrystals and graphene quantum dots for detection of trace Iron(III), ACS Appl. Nano Mater. 6 (13) (2023) 11561–11571, https://doi.org/10.1021/acsanm.3c01584.
[52] S. Lee, B.-H. Jun, Silver nanoparticles: synthesis and application for nanomedicine, Int. J. Mol. Sci. 20 (4) (2019) 865, https://doi.org/10.3390/ijms20040865.
[53] K.B.R. Teodoro, M.J. Silva, R.S. Andre, R. Schneider, M.A. Martins, L.H.C. Mattoso, D.S. Correa, Exploring the potential of cellulose autofluorescence for optical detection of tannin in red wines, Carbohydr. Polym. 324 (2024) 121494, https://doi.org/10.1016/j.carbpol.2023.121494.
[54] Y. Peng, B. Via, The effect of cellulose nanocrystal suspension treatment on suspension viscosity and casted film property, Polymers 13 (13) (2021) 2168, https://doi.org/10.3390/polym13132168.
[55] A. Beélik, J.K. Hamilton, The ultraviolet irradiation of model compounds related to cellulose [1], J. Organomet. Chem. 26 (12) (1961) 5074–5080, https://doi.org/10.1021/jo01070a071.
[56] G. Biliuta, S. Coseri, Cellulose: A ubiquitous platform for ecofriendly metal nanoparticles preparation, Coord. Chem. Rev. 383 (2019) 155–173, https://doi.org/10.1016/j.ccr.2019.01.007.
[57] D. Huang, M. Wu, S. Kuga, Y. Huang, Size-controlled silver nanoparticles supported by pyrolytic carbon from microcrystalline cellulose, Int. J. Mol. Sci. 24 (19) (2023) 14431, https://doi.org/10.3390/ijms241914431.

[58] A. Zeng, R. Yang, Y. Tong, W. Zhao, Functional bacterial cellulose nanofibrils with silver nanoparticles and its antibacterial application, Int. J. Biol. Macromol. 235 (2023) 123739, https://doi.org/10.1016/j.ijbiomac.2023.123739.
[59] M.F. Cortes Ruiz, Y. Brusentsev, S.B. Lindström, C. Xu, L. Wågberg, Shape-recovering nanocellulose networks: preparation, characterization and modeling, Carbohydr. Polym. 315 (2023) 120950, https://doi.org/10.1016/j.carbpol.2023.120950.
[60] A.G.N. Sofiah, J. Pasupuleti, M. Samykano, K. Kadirgama, S.P. Koh, S.K. Tiong, A. K. Pandey, C.T. Yaw, S.K. Natarajan, Harnessing nature's ingenuity: A comprehensive exploration of Nanocellulose from production to cutting-edge applications in engineering and sciences, Polymers 15 (14) (2023) 3044, https://doi.org/10.3390/polym15143044.
[61] ICH, C. de D, ICH topic Q2 (R1) validation of analytical procedures : text and methodology, International Conference on Harmonization, 2005. http://www.ich.org/fileadmin/Public_Web_Site/ICH_Products/Guidelines/Quality/Q2_R1/Step4/Q2_R1__Guideline.pdf.
[62] M.-M. Liu, X. Lian, H. Liu, Z.-Z. Guo, H.-H. Huang, Y. Lei, H.-P. Peng, W. Chen, X.-H. Lin, A.-L. Liu, X.-H. Xia, A colorimetric assay for sensitive detection of hydrogen peroxide and glucose in microfluidic paper-based analytical devices integrated with starch-iodide-gelatin system, Talanta 200 (2019) 511–517, https://doi.org/10.1016/j.talanta.2019.03.089.
[63] R. Bandi, M. Alle, C.-W. Park, S.-Y. Han, G.-J. Kwon, N.-H. Kim, J.-C. Kim, S.-H. Lee, Cellulose nanofibrils/carbon dots composite nanopapers for the smartphone-based colorimetric detection of hydrogen peroxide and glucose, Sens. Actuators B 330 (2021) 129330, https://doi.org/10.1016/j.snb.2020.129330.
[64] Y. Mirzaei, A. Gholami, A. Sheini, M.M. Bordbar, An origami-based colorimetric sensor for detection of hydrogen peroxide and glucose using sericin capped silver nanoparticles, Sci. Rep. 13 (1) (2023) 1–10, https://doi.org/10.1038/s41598-023-34299-1.
[65] N. Srikhao, A. Ounkaew, P. Kasemsiri, S. Theerakulpisut, M. Okhawilai, S. Hiziroglu, Green synthesis of silver nanoparticles using the extract of spent coffee used for paper-based hydrogen peroxide sensing device, Sci. Rep. 12 (1) (2022) 20099, https://doi.org/10.1038/s41598-022-22067-6.
[66] B.N. Khlebtsov, A.M. Burov, A.M. Zakharevich, N.G. Khlebtsov, SERS and Indicator paper sensing of hydrogen peroxide using au@ag Nanorods, Sensors 22 (9) (2022) 3202, https://doi.org/10.3390/s22093202.
[67] S. Kwon, S. Ko, Colorimetric freshness indicator based on cellulose nanocrystal–silver nanoparticle composite for intelligent food packaging, Polymers 14 (17) (2022) 3695, https://doi.org/10.3390/polym14173695.
[68] J. Otsuki, K. Sugawa, S. Jin, Plasmonic triangular nanoprism sensors, Mater. Adv. 2 (1) (2021) 32–46, https://doi.org/10.1039/D0MA00644K.
[69] Y. Wang, Y. Yang, W. Liu, F. Ding, Q. Zhao, P. Zou, X. Wang, H. Rao, Colorimetric and fluorometric determination of uric acid based on the use of nitrogen-doped carbon quantum dots and silver triangular nanoprisms, Microchim. Acta 185 (6) (2018), https://doi.org/10.1007/s00604-018-2814-6.
[70] J.G. Mahy, M. Kiendrebeogo, A. Farcy, P. Drogui, Enhanced decomposition of H2O2 using metallic silver nanoparticles under UV/visible light for the removal of p-Nitrophenol from water, Catalysts 13 (5) (2023) 842, https://doi.org/10.3390/catal13050842.